JOURNAL OF APPLIED ELECTROCHEMISTRY 23 (1993) 1089–1096

# First stages of the formation of copper electrodeposits and copper sputtered deposits on amorphous carbon and polycrystalline silver substrates

P. VANDEN BRANDE, R. WINAND

*Université Libre de Bruxelles, Department Metallurgy-Electrochemistry, CP 165, 50 Avenue F.D. Roosevelt, B1050 Brussels, Belgium*

Received 25 November 1992; revised 18 February 1993

The first stages of the development of copper deposits on amorphous carbon and polycrystalline silver substrates are compared when the deposits are produced by electrodeposition under galvanostatic conditions and by high rate magnetron-enhanced sputtering. It is shown that the first stages of the formation of the metallic deposits are influenced by the deposition rate, the substrate-to-deposit interaction and by the deposition technique. These factors have a particular influence on the growth mode and on the nucleation stage of the deposit. When an island growth mode is observed, an increase of the deposition rate induces thinner covering films because the island density is higher and the islands are smaller for a given quantity of deposited matter. In electrodeposition, an island growth mode is observed on the two types of substrate, but for equivalent experimental conditions the superficial cluster density is higher on silver than on carbon substrates. Dissolution of some copper clusters occurs a short time after the onset of electrolysis. This can be explained by local changes of the supersaturation due to a current microdistribution at the cathode surface. In magnetron-enhanced sputtering, an island growth mode is observed on amorphous carbon substrates, while a layer-by-layer growth mode is detected on polycrystalline silver substrates. On silver substrates two different growth modes are thus observed depending on the deposition technique. In contrast, on carbon substrates, where an island growth mode is observed in both cases, the copper cluster superficial density is a factor $10^6$ to $10^8$ higher in sputtering than in electrodeposition for the same deposition rate. This paper shows that these differences can only be explained by physical and chemical mechanisms specific to each deposition technique taking place during the condensation process.

## 1. Introduction

In two previous papers the importance of the influence of the deposition rate and the deposit-to-substrate interaction on the first stages of the formation of copper electrodeposits [1] and copper sputtered deposits [2] has been shown. The deposition rate and the substrate nature have, in particular, an influence on the growth mode and the nucleation stage of the deposit.

The nucleation rate and the cluster critical size of the newly formed metallic deposit are functions of the supersaturation which measures the energetic gap between the out-of-equilibrium bulk metallic phase [3, 4]. In electrodeposition, the supersaturation $\Delta G$ depends on the cathodic overvoltage, $\eta$, and on the electrical charge, $ze$, ($z$: number of exchanged electrons, $e$: electronic charge) necessary to discharge one ion

$$\Delta G = -ze\eta \qquad (1)$$

In sputtering, and more generally in physical vapour deposition, the supersaturation is a function of the pressure ratio $P/P_\infty$, where $P$ corresponds to the substrate atomic bombardment flow and $P_\infty$ is the vapour pressure of the bulk phase at the substrate temperature $T$. Accordingly,

$$\Delta G = kT \ln (P/P_\infty) \qquad (2)$$

where $k$ is the Boltzmann constant.

The cluster critical size which corresponds to the maximum cluster free energy (or the size for which the cluster growth probability is higher than the cluster decay probability), for a given supersaturation, is proportional to $\sigma^3/\Delta G^3$, where $\sigma$ is the cluster mean specific superficial energy. When the supersaturation increases, the cluster critical size decreases and, in practice, is lower than a few atoms. Generally a single adatom can be considered as critical or supercritical [5–7]. Information on the nuclei generally comes from the interpretation of the cluster density distribution as a function of time (or the quantity of deposited matter) via a nucleation model. This model is, in practice, necessarily atomistic and not capillary, because for very small clusters some thermodynamic properties, e.g. the specific surface energy and the free energy, lose their physical meaning.

0021-891X © 1993 Chapman & Hall

The growth mode depends mainly on the deposit-to-substrate interaction compared with the deposit cohesion. Let $E_a$ be the deposit atomic adsorption energy and $E_c$ the deposit atomic cohesion energy. Two very different situations can be observed: the first, when $E_a < E_c$, induces an island growth mode (Volmer–Weber) while the second, for which $E_a > E_c$, corresponds to a layer-by-layer growth process (Frank–van der Merwe). The first situation where $E_a < E_c$ can be induced on an amorphous carbon substrate because of the weak bonding between carbon and copper. The second situation where $E_a > E_c$ can only be approached on a polycrystalline silver substrate because the bonding between the substrate and the deposit is a metallic bonding so that $E_a$ should be in the same range as $E_c$.

The first stages of the formation of copper electrodeposits [1] and copper sputtered deposits [2] on amorphous carbon and polycrystalline silver substrates against the deposition rate present differences for equivalent deposition rates and on substrates of the same nature. These differences are consequently due to the deposition techniques.

The aim of this paper is to show how the deposition rate, the substrate nature and the deposition technique can influence the first stages of the formation of a copper deposit and to discuss the main differences observed between electrodeposits and sputtered deposits.

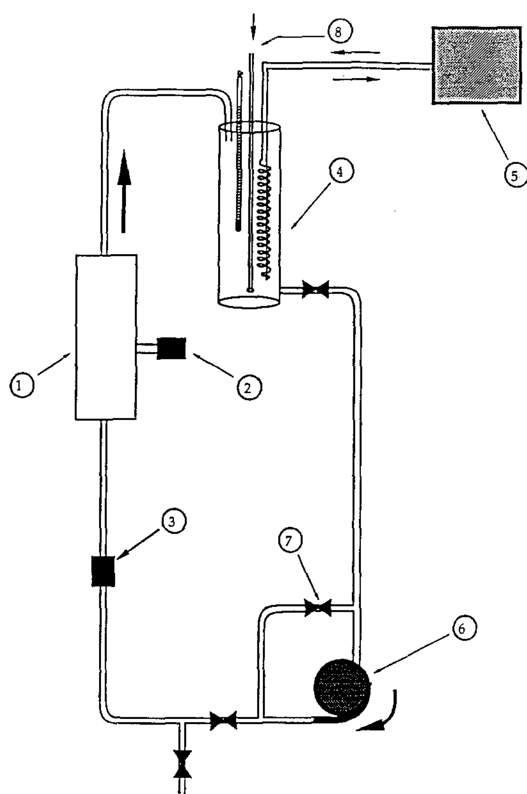


Fig. 1. Overview of the electrolyte flow circuit of the electrolysis cell: (1) electrolytic flow through channel cell; (2) reference electrode; (3) flowmeter; (4) electrolyte tank; (5) thermostat; (6) centrifugal pump; (7) bypass; (8) nitrogen inlet.

## 2. Experimental methods

### 2.1. *Galvanostatic electrodeposition technique*

Galvanostatic conditions were achieved in a flow through channel cell which allowed good reproducibility for the hydrodynamical conditions (Fig. 1). The flow speed was $2\,m\,s^{-1}$ in front of the cathode. The electrolyte was a solution of 0.5 M $CuSO_4$ and $20\,g\,dm^{-3}$ $H_2SO_4$ deaerated by nitrogen flow. Its temperature was regulated at 298 K by a secondary water flow circuit. The anode was made of copper.

To be able to use transmission electron microscopy (TEM) to study small copper crystallites, a deposition technique on thin film substrates of a layered type was developed (Fig. 2). The first layer was a silver conducting layer of about 50 nm. If the substrate surface was made of amorphous carbon, a 10 nm carbon layer lay on the silver layer. The mechanical support of the film substrate was a glass plate. The thickness of the film substrate was large enough for it to be an equipotential under the chosen experimental conditions and small enough to be transparent to electrons in TEM. The different layers which constitute the substrate were deposited by vacuum vapour deposition on the glass plate.

### 2.2. *Copper sputtering deposition technique*

The substrates and deposits were prepared in the same vacuum vessel a Leybold L560 magnetron-enhanced sputtering machine.

Before each experiment, the vacuum chamber was pumped down to a vacuum of $10^{-6}$ torr, in order to deposit by vacuum evaporation either a polycrystalline silver film or an amorphous carbon film on a glass plate. These films constitute the substrates on which the copper sputtered deposits were produced.

After production, the substrate was moved under vacuum (by means of a rotative substrate holder) and placed in front of the sputtering target. The pressure was then increased to $5 \times 10^{-3}$ torr by inlet

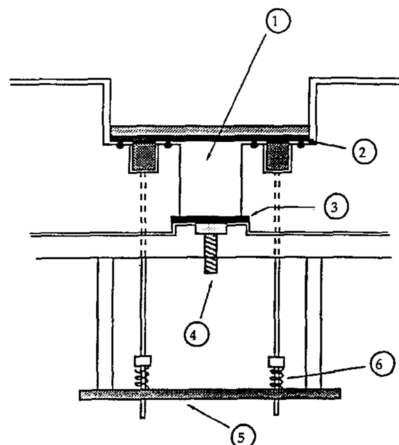


Fig. 2. Cross-section of the electrodeposition cell for thin film substrates: (1) electrolyte channel; (2) thin conducting film (cathode); (3) anode; (4) anode current lead; (5) cathode current lead; (6) spring.

*Table 1. Sputtering parameters*

| *Target current*/A | *Dep. rate*/atoms $s^{-1}$ $cm^{-2}$ | *Target voltage*/V |
|---|---|---|
| 0.1 | $4.2 \times 10^{15}$ | −310 |
| 0.5 | $21.2 \times 10^{15}$ | −370 |
| 2 | $93.7 \times 10^{15}$ | −480 |

of high purity argon in the vacuum chamber. Because the substrate surface was intrinsically as clean as possible under this argon pressure, no other pretreatment procedure was performed.

The d.c. plasma was then induced under $5 \times 10^{-3}$ torr of argon for a copper-target-to-substrate distance of 55 mm. The deposition rate was constant and regulated by the target current. The substrate temperature was measured by a thermocouple placed on the substrate holder, close to the silver or carbon film (room temperature). The target voltage increased with the deposition rate which is a function of the target current. The experimentally determined correspondence between the target current, the deposition rate and the target voltage (relative to the ground potential) is shown in Table 1.

### 2.3. *Analytical techniques*

Copper electrodeposits were directly observed by scanning electron microscopy (SEM) and TEM when a higher resolution was needed. Pictures of the deposits (clusters on the substrate) were digitized and introduced to a computer for analysis by a specially developed program [3]. In this way, information was obtained on the evolution of cluster size, cluster surface density and cluster surface distribution. The results were compared with the chemically measured copper deposited quantities (by atomic absorption spectroscopy after dissolution of the deposit in nitric acid). These last results also allowed the determination of the current efficiency.

The characterization of the first stages of the formation of copper sputtered deposits was not possible by SEM, because of a lack of resolution, and by TEM because the contrasts were not sufficient and the deposits were damaged by the high energy (100 keV) electronic bombardment in the microscope. This electronic bombardment created a recrystallization process during the observation [2]. To solve this problem, the observation had to be done by a lower energy analysis technique like Auger electron spectroscopy (AES). It has been shown previously [2, 3] that the observation of the deposit by this technique at different stages of growth can, with the help of a model, give information on its growth mode.

The deposit-to-substrate Auger peak-to-peak intensity ratio is usually related to the number of deposited atoms by means of three growth models: the island or Volmer–Weber growth mode, the layer-by-layer or Frank–van der Merwe growth mode and, finally, the coalescence of clusters mode. Each of these models is valid only within certain limits: the beginning of the film formation for the first and the second models and after the beginning of coalescence for the third model. These models each present a characteristic evolution of the deposit-to-substrate Auger peak-to-peak intensity ratio, $R$, against the quantity of deposited matter, $e$, expressed as the equivalent number of atomic monolayers, as shown in Fig. 3. The Frank–van der Merwe model leads to a rapid change of $R$ against $e$. On the other hand, the Volmer–Weber model leads quite rapidly to a constant maximum $R$ value, corresponding to the covering fraction ($x$) of the substrate by the islands, which is assumed constant when the nucleation stage is complete and before the coalescence stage of clusters. It is therefore possible, comparing the experimental data with the theoretical curves, to confirm or deny the presence of these growth modes. In the case of an island growth mode, when the uncovered substrate surface fraction becomes small enough, it is no longer possible to neglect the lateral growth of the islands and the model becomes ineffective: the higher the $e$, the more the experimental data deviate from the theoretical curves. It is therefore necessary to consider the third model: the cluster coalescence model, where $R$ increases according to $e$ as the uncovered substrate surface fraction tends to zero.

The characteristic of an island growth mode is thus the presence of the Volmer–Weber model plateau. In this zone, the attenuation of the substrate Auger signal screened by the islands is complete. In practice, this situation occurs when the island height is more than ten atomic layers. The result is a constant Auger deposit-to-substrate peak-to-peak intensity ratio $R$ against $e$, because the Auger deposit signal and the Auger substrate signal (which derives from the uncovered substrate surface) are constant, due to the constant covering fraction, $x$, of the deposit. This assumption is valid only if the apparent surface area of the islands increases slowly when compared to the covered substrate surface fraction and to the uncovered substrate surface fraction (then,

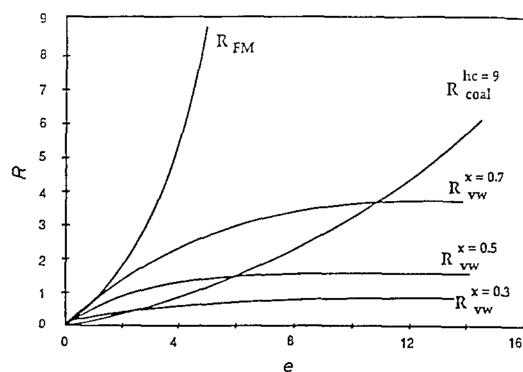


Fig. 3. Theoretical deposit (copper) to substrate (carbon) Auger peak-to-peak intensity ratio $R$ as a function of $e$, the quantity of deposited matter per area unit expressed as the equivalent number of atomic monolayers for three models: Frank–van der Merwe (FM), Volmer–Weber (VW) and coalescence (Coal) where $h_c$ is the cluster mean height at the beginning of coalescence. Only one curve is obtained for the Frank–van der Merwe growth mode; however, one curve is obtained for each $x$ value in the Volmer–Weber growth mode.

*Table 2. Equivalence table between the current density J and the deposition rate q*

| $J$/A dm$^{-2}$ | $q$/atom s$^{-1}$ cm$^{-2}$ |
|---|---|
| 0.134 | $4.1 \times 10^{15}$ |
| 0.68 | $21.2 \times 10^{15}$ |
| 3.0 | $93.7 \times 10^{15}$ |

obviously, this can only be true when $x$ is not very small nor very high). This assumption means, in fact, that the lateral growth of the islands is neglected.

Given the values of $R$ and $e$ on the plateau, if an island growth mode is observed, it is possible to calculate the value of the deposit covering fraction $x$, an estimation of the mean apparent area of a cluster and the cluster mean superficial density [2].

More details about the derivation of the Auger models for each growth mode, the quantitative Auger analysis and the estimations of the mean cluster density and of the cluster mean apparent area are given in [2].

### 2.4. *The equivalence between the current density, J, in electrodeposition and the deposition rate q in sputtering*

To compare the first stages of the formation of copper deposits on a given substrate (carbon or silver) and for equivalent deposition rates by electrodeposition and by sputtering, it is necessary to establish the equivalence between the current density, $J$, and the deposition rate, $q$. The deposition rate $q$ corresponding to the current density, $J$, is the number of ions discharged on the substrate surface (cathode) per unit area and unit time. The correspondence between $J$ and $q$ is given in Table 2.

## 3. Experimental results

### 3.1. *Copper electrodeposits on amorphous carbon substrates*

An island growth mode was observed for current densities varying from 0.134 A dm$^{-2}$ to 10 A dm$^{-2}$. The results are given for 0.134 A dm$^{-2}$.

Figure 4 shows the relation between the current efficiency, $r_c$, the cluster superficial density, $N$, the

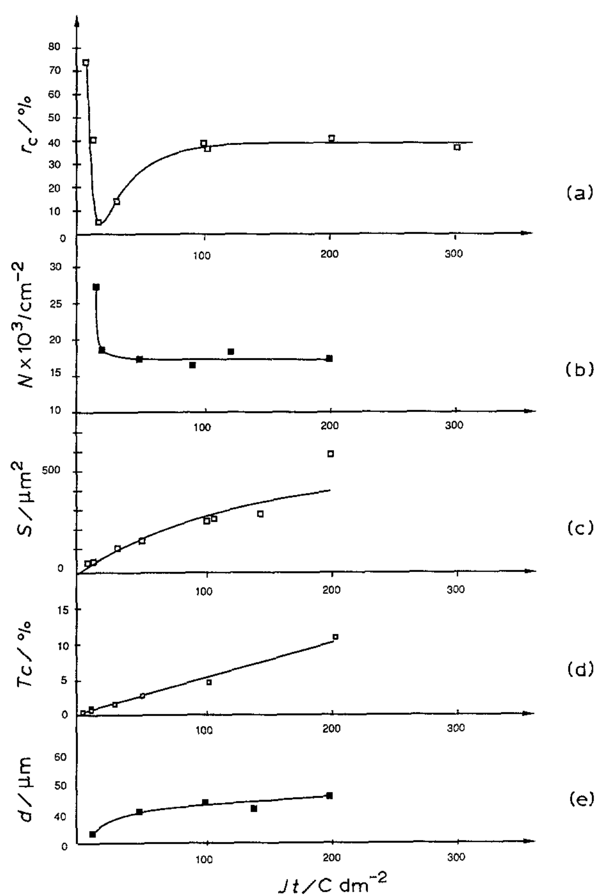


Fig. 4. Parallel evolution of the current efficiency $r_c$, cluster superficial density $N$, cluster mean apparent surface $S$, covering ratio $Tc$ and nearer-neighbour cluster mean distance $d$ against the quantity of electricity $J \times t$, for copper electrodeposited on an amorphous carbon substrate ($J = 0.134$ A dm$^{-2}$).

cluster mean size or apparent area, $S$, the covering ratio, $T_c$, and the nearer-neighbour cluster mean distance, $d$, against the quantity of electricity $Jt$. The current efficiency presents a minimum in a first zone and a constant value in a second zone (Fig. 4a). The decrease of $r_c$ in the first zone corresponds to a decrease in $N$ (Fig. 4b) and an increase in $d$ (Fig. 4e) while in the second zone, the constant value of $r_c$ is related to the constant value of $N$ and to the constant value of $d$. The cluster mean apparent area $S$ (Fig. 4c) and the covering ratio $T_c$ (Fig. 4d) increase monotonically against $Jt$.

The generally low current efficiency is linked to the low covering ratio [1]. When the covering ratio

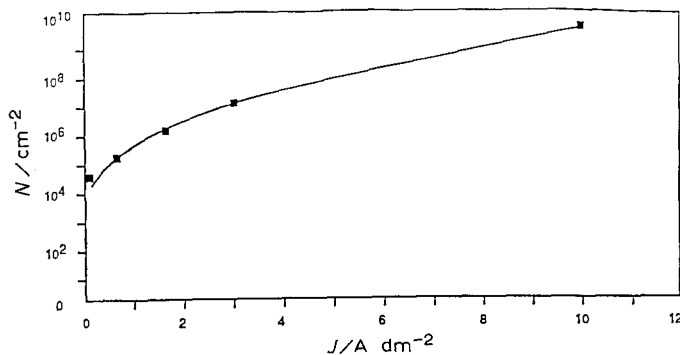


Fig. 5. Cluster surface density $N$ against the current density $J$ at the beginning of coalescence for copper electrodeposits on amorphous carbon substrates.

*Table 3. Cathodic overvoltage $\eta$ and calculated supersaturation $\Delta G$ against J*

| $J$/A dm$^{-2}$ | $\eta$/mV | $\Delta G$/eV |
|---|---|---|
| 0.134 | −210 | 0.42 |
| 0.68 | −290 | 0.58 |
| 3.0 | −360 | 0.72 |

reaches 100%, the current efficiency increases to values near 100%. Globally, when the current density increases, the current efficiency increases, the cluster superficial density increases (Fig. 5), the cluster mean size decreases and the nearer-neighbour cluster mean distance decreases [1].

The measured overvoltage, in the initial stages of the electrodeposition process, was proved to be characteristic of the degree of supersaturation of the system because, due to the high electrolyte velocity in front of the cathode, only a charge transfer-crystallization process without diffusion was observed at the cathode [3]. Table 3 presents the evolution of the cathodic overvoltage $\eta$ and of the calculated supersaturation, $\Delta G$, according to Equation 1, at the beginning of the deposition process, against the current density $J$ ($z = 2$). It is shown that the absolute value of the cathodic overvoltage and the supersaturation increase against $J$.

### 3.2. *Copper electrodeposits on polycrystalline silver substrates*

On polycrystalline silver substrates an island growth mode was detected similarly to similar experiments performed on amorphous carbon substrates [3]. For instance, the current efficiency curves against $Jt$ (at given $J$) show a minimum, but less pronounced than on carbon substrates. For $J = 0.68$ A dm$^{-2}$, the minimum value of the current efficiency $r_c$ is equal to 50% on a silver substrate while the minimum value of the current efficiency is 30% on a carbon substrate.

Meanwhile, the surface density of clusters, $N$, is higher and the cluster mean size, $S$, is smaller on silver substrates than on carbon substrates, for an equivalent current density at the beginning of the coalescence, as illustrated in Table 4.

### 3.3. *Copper sputtered deposits on amorphous carbon substrates*

The normalized copper-to-carbon Auger peak-to-peak intensity ratio, $R$, against the deposited quantity of matter, $e$, is presented (Fig. 6) for three different values of the deposition rate. All these curves are similar. An increase of the deposition rate implies a higher $R$ value given the $e$ value. Each curve has three zones: the first where an increase of $R$ against $e$ is observed, the second characterized by a plateau where $R$ is constant with changing $e$ (characteristic of an island growth mode) and the third zone with a rapid increase of $R$ against $e$ (coalescence of clusters). Using a model developed elsewhere [2, 3], it is possible to calculate the covering ratio, $x$, the mean apparent area, $S$, of a cluster and the mean cluster superficial density, $N$, for each of the three curves, given the $R$ and $e$ values. The results are summarized in Table 5, assuming a cubic geometry for the clusters. More details of these derivations are given in [2].

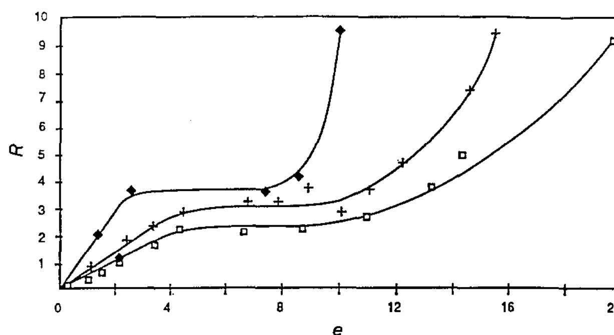

Fig. 6. Normalized experimental deposit-to-substrate Auger peak-to-peak intensity ratio $R$ as a function of $e$ the number of equivalent deposited atomic layers of copper sputtered on a carbon substrate for three deposition rates. (□) $4.2 \times 10^{15}$ atom s$^{-1}$ cm$^{-2}$; (+) $21.2 \times 10^{15}$ atom s$^{-1}$ cm$^{-2}$; (◆) $93.7 \times 10^{15}$ atom s$^{-1}$ cm$^{-2}$.

From Table 5 it can be concluded that an increase in the deposition rate induces an increase in the cluster surface density and a decrease in the cluster mean apparent area.

### 3.4. *Copper sputtered deposits on polycrystalline silver substrates*

The results for the two deposition rates ($q = 4.2 \times 10^{15}$ cm$^{-2}$ s$^{-1}$ and $q = 21.2 \times 10^{15}$ cm$^{-2}$ s$^{-1}$ presented in Fig. 7 show that $R$ increases with $e$ in both cases. This is probably due to a Frank–van der Merwe growth mode. It is obvious that, in this case, the Volmer–Weber growth process must be rejected. More details about this conclusion, are given in [2].

*Table 4. Comparison between the cluster surface density N and the cluster mean apparent area S for copper electrodeposits on silver and carbon substrates at the beginning of the coalescence*

| | Silver substrates | | Carbon substrates | |
|---|---|---|---|---|
| $J$/A dm$^{-2}$ | $N$/cm$^{-2}$ | $S$/$\mu$m$^2$ | $N$/cm$^{-2}$ | $S$/$\mu$m$^2$ |
| 0.68 | $3 \times 10^8$ | 0.18 | $10^5$ | 100 |
| 3.0 | $> 12 \times 10^8$ | 0.03 | $10^7$ | 1 |

*Table 5. Covering ratio x, mean apparent area S and mean cluster superficial density N against the deposition rate q calculated on the basis of R and e values taken in the middle of the plateau of the three curves of Fig. 6*

| $q$/cm$^{-2}$ s$^{-1}$ | $R$ | $e$ | $x$/% | $S$/(nm)$^2$ | $N$/cm$^{-2}$ |
|---|---|---|---|---|---|
| $4.2 \times 10^{15}$ | 2.14 | 8 | 62 | 8.58 | $7.2 \times 10^{12}$ |
| $21.2 \times 10^{15}$ | 2.86 | 7 | 68 | 5.48 | $12.4 \times 10^{12}$ |
| $93.7 \times 10^{15}$ | 3.43 | 6 | 72 | 3.53 | $20.4 \times 10^{12}$ |

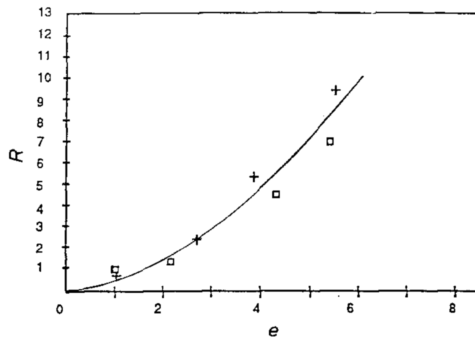


Fig. 7. Normalized experimental deposit-to-substrate Auger peak-to-peak intensity ratio $R$ as a function of $e$ the number of equivalent deposited atomic layers of copper sputtered on a silver substrate for two deposition rates. (□) $4.2 \times 10^{15}$ atom $s^{-1}$ $cm^{-2}$; (+) $21.2 \times 10^{15}$ atom $s^{-1}$ $cm^{-2}$.

## 4. Discussion

### 4.1. *Copper electrodeposits*

The observed current efficiency decrease at very short electrolysis duration corresponds to the decrease of the cluster surface density. This means that a significant copper loss occurs during the first stages of the electrodeposition process. It was shown in a previous paper [1] that these clusters disappear principally in zones lying around bigger islands, so-called exclusion zones, because of a dissolution process explained by local changes of the supersaturation due to a current microdistribution at the cathode surface. The presence of exclusion zones of this type was described in the literature [8–10]. Later, during the electrodeposition process, the cluster density becomes constant and the clusters grow until coalescence. The current efficiency reaches 100% only when the covering ratio reaches 100%, which is usual in copper electrodeposition. When the deposit is constituted by discrete islands and the covering ratio is lower than 100%, the dissolution effect plays an important role because the current efficiency is lower than 100%. The observed constant value of the cluster superficial density (at given $J$) is thus not representative of the initial nuclei distribution which was much higher before the dissolution process became important. However, on an amorphous carbon substrate, the cluster superficial density (at a given deposition rate) is $10^6$ to $10^8$ higher in copper sputtering condensation than in copper electrodeposition. At the supersaturation level experimentally observed (cf. Table 3) an atomistic nucleation process is highly probable in the early stages of the film formation. This should lead, in the absence of the dissolution process, to a higher cluster density than that experimentally observed, with a magnitude similar to that observed in physical condensation. The large discrepancy indicates the importance of the cluster dissolution process during electrodeposition. A model for this process was previously proposed [1]. When an island grows, the current flow lines and the pattern of the equipotentials in the electrolyte change. This induces a decrease in the current density and also a decrease in the overvoltage around the island. A small cluster, supercritical outside where no large island is growing, can become subcritical in the vicinity of such a large growing island. This subcritical cluster dissolves in the electrolyte (Fig. 8), resulting in the above-mentioned exclusion zone around the big island. This special behaviour in the first stages of the formation of a copper electrodeposit illustrates the importance of the chemical and physical processes taking place during the condensation process and linked to the deposition technique.

On carbon, as well as on silver substrates, an increase in the current density induces an increase in the cluster surface density, a higher covering ratio and an increase in the supersaturation, as shown in Table 3. The cluster surface density probably increases because the clusters are more stable for higher values of the supersaturation (linked to the decrease in the dissolution process when $J$ increases) and because if the supersaturation increases, the nucleation rate also theoretically increases [3].

On silver substrates, the cluster surface density is higher and the cluster mean size is smaller than on carbon substrates under equivalent experimental conditions, probably because the higher adhesion energy between copper and silver than between

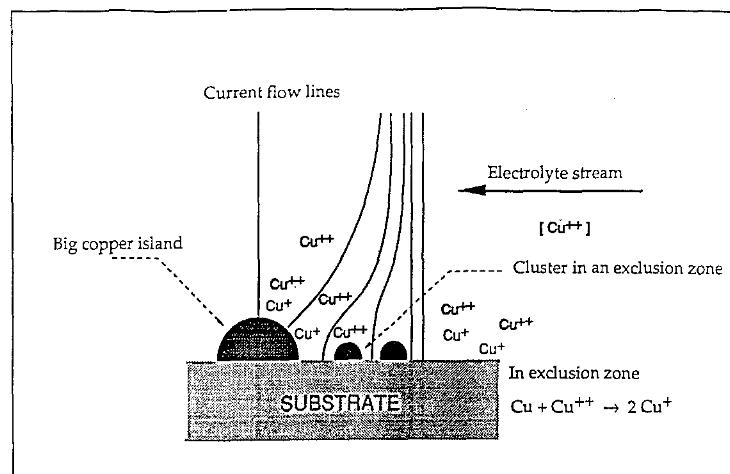


Fig. 8. Schematic process of the dissolution of a copper cluster in the exclusion zone of a big copper island during electrodeposition. In the exclusion zone, $Cu + Cu^{2+} \rightleftharpoons 2Cu^{+}$.

copper and carbon stabilizes the clusters. On the other hand, when the adhesion energy increases, the supersaturation being constant, the nucleation rate theoretically increases [3, 4]. This shows the importance of the deposit-to-substrate interaction on the first stages of the deposit formation. The authors believe that most experimental results described in the literature concerning instantaneous or progressive nucleation deal, in fact, with clusters observed after the exclusion zones are generated.

### 4.2. *Copper sputtered deposits*

An increase of the deposition rate induces an increase in the cluster surface density and a decrease in the cluster apparent area on an amorphous carbon substrate through an increase in the nucleation rate linked to the increase in the supersaturation as shown by Formula 2.

A carbon substrate induces a copper island growth mode while on a silver substrate a layer-by-layer growth mode is observed due to an increase in the atomic adsorption energy. Some authors [11] have observed a Stranski–Krastanov growth mode, which is an intermediate form between a Volmer–Weber and a Frank–van der Merwe growth mode. In the Stranski–Krastanov growth mode, after completion of a first monoatomic layer deposit, there is an island growth mode due to the decrease of the adsorption energy. The reason for the difference between the growth process observed in this paper and that described in the literature may be the high kinetic energy of the sputtered copper atoms which is probably sufficiently high to create defects on the substrate surface, increasing the adsorption energy per adatom on the substrate surface so that $E_a > E_c$. This proves the influence of the deposit-to-substrate interaction on the first stages of the development of the sputtered deposit.

Depending on the deposition technique, on silver substrates and at the same deposition rate, a layer-by-layer growth mode is observed in sputtering while an island growth mode is observed in electrodeposition. This difference can only be attributed to the different chemical and physical mechanisms taking place during the condensation process for each one of the deposition techniques.

## 5. Conclusion

This paper shows that the first stages of the formation of a copper deposit depend on the deposition rate, the substrate surface nature and the deposition technique.

When an island growth mode is observed, whatever the deposition technique, an increase in the deposition rate induces thinner covering films, partially because the nucleation rate increases. On a carbon substrate, island growth modes are observed both in electrodeposition and in sputtering. In contrast, on a silver substrate, an island growth mode is still detected in electrodeposition while a layer-by-layer growth mode is observed in sputtering. This illustrates the importance of the physical and chemical mechanisms taking place during the deposition process for each deposition technique.

Models for the first stages of the formation of copper deposits by electrodeposition and by sputtering, on amorphous carbon and polycrystalline silver substrates, can be derived from the experimental results.

In electrodeposition, on carbon and silver substrates, the local deposition rate is variable on the substrate surface (effect of the current microdistribution due to the cathodic surface microgeometry) and explains the local changes of the supersaturation. The decrease of the supersaturation in exclusion zones around big islands induces the dissolution of small clusters. This phenomenon occurring at the beginning of the film formation results in a minimum

*Table 6. Influence of the deposition technique on the first stages of the deposit formation*

| | *Sputtering* | *Electrodeposition* |
|---|---|---|
| Substrate local deposition Rate | Uniform | Function of the substrate local microgeometry |
| Substrate local supersaturation | Uniform and in the range of some eV | Function of the substrate local microgeometry but less than some 0.1 eV |
| Cluster critical size corresponding to the mean value of the supersaturation | 1: a single adatom is at least critical | 1: a single adatom is at least critical |
| Current efficiency | | < 100% and presents a min. against $Jt$ ($J$ is constant). Cluster dissolution is observed in so-called 'exclusion zones' |
| Growth mode | | |
| $E_a \approx E_c$ (on Ag substrates) | Frank–van der Merwe | Stranski–Krastanov followed by ion incorporation in clusters (cluster growth) and cluster coalescence |
| $E_a < E_c$ (on C substrates) | Volmer–Weber followed by cluster coalescence | Volmer–Weber followed by ion incorporation in clusters (cluster growth) and cluster coalescence |

in the current efficiency curve against $Jt$ at constant current density. The calculated supersaturation is theoretically high enough to make single adatoms supercritical. After the initial nucleation stage, not accessible to experiment, the clusters are subject to growth by direct ions discharge and to dissolution if they enter the exclusion zones of bigger islands. This leads quite rapidly to a constant surface density of growing islands until they coalesce.

In sputtering, the local deposition rate is constant over the substrate surface. The supersaturation, which can be calculated by Formula 2, is approximately 2.5 eV [3] and is constant over the substrate surface. For this supersaturation value a single adatom is supercritical and the sticking coefficient can be considered as very close to one on a cold substrate [3, 4]. On a silver substrate a Frank–van der Merwe growth mode is observed because the kinetic energy of the impinging sputtered atoms is high enough to create defects on the substrate and deposit surface. These defects increase artificially the atomic adsorption energy per adatom so that $E_a > E_c$ in this case. The silver substrate is perfectly covered by one deposited equivalent atomic layer. On a carbon substrate where a Volmer–Weber growth mode followed by coalescence is detected, the experimental results show that more than 20 deposited equivalent atomic layers are needed to produce a perfectly covering film. Table 6 summarizes the influence of the deposition technique on the first stages of the deposit formation.

**Acknowledgements**

The authors thank l'Institut pour l'Encouragement à la Recherche Scientifique dans l'Industrie et l'Agriculture and the National Fund for Scientific Research, two Belgian governmental organizations, for partial financial support.

**References**

[1] P. Vanden Brande and R. Winand, *Surf. & Coatings Technol.* **52** (1992) 1.
[2] *Idem, ibid.* **52** (1992) 9.
[3] P. Vanden Brande, Ph.D. Thesis, Université Libre de Bruxelles (1990).
[4] B. Lewis and J. C. Anderson, 'Nucleation and Growth of Thin Films', Academic Press, New York (1978).
[5] G. Zinsmeister, *Thin Solid Films* **2** (1968) 497.
[6] A. Milchev, *Electrochim. Acta* **28** (1983) 947.
[7] A. Milchev and S. Stoyanov, *J. Electroanal. Chem.* **72** (1976) 33.
[8] G. Adzic, A. R. Despic and D. M. Drazic, *ibid.* **220** (1987) 169.
[9] E. A. Mamontov, L. A. Kurbatova and A. P. Volenko, *Elektrokhimiya* **23** (1987) 187.
[10] I. Markov, A. Boynov and S. Toschev, *Electrochim. Acta* **18** (1973) 377.
[11] H. Ke, X. Li, A. Zhang and Z. Qi, *Phys. Lett. A* **136** (1989) 445.